ELSEVIER

Surface Science 425 (1999) 68–80

surface science

Dependence of stretching frequency on surface coverage and adsorbate–adsorbate interactions: a density-functional theory approach of CO on Pd (111)

D. Loffreda, D. Simon, P. Sautet *

Institut de Recherches sur la Catalyse, Centre National de la Recherche Scientifique, 2 Avenue Albert Einstein, Villeurbanne Cedex 69626, France

Laboratoire de Chimie Théorique, Ecole Normale Supérieure de Lyon, 46 Allée d'Italie, Lyon 69364 Cedex 07, France

Received 27 November 1998; accepted for publication 15 January 1999

Abstract

Total energy and stretching frequency calculations ν(C–O) are reported for the chemisorption of CO on a Pd (111) surface as a function of coverage with a periodic density-functional theory approach including generalized gradient approximation. At low [0.33 monolayer (ML)] and high (0.75 ML) coverages, the most stable structures always present CO in threefold fcc and hcp hollow sites, mixed with top sites for the high coverage structure, in agreement with the interpretation of the RAIRS or HREELS spectra. The calculated anharmonic frequencies for these sites (1828–1830 cm^{-1} at 0.33 ML) and (1893 and 2085 cm^{-1} at 0.75 ML) are coherent with the observed IR peaks. At medium coverage, 0.5 ML, the most stable model is the one with both fcc and hcp hollow sites. The observed blue shift of the frequency band between 0.33 ML and 0.5 ML is usually interpreted as a change of the chemisorption site from a hollow to a bridge adsorption. Although a direct comparison of the IR peak with the calculated anharmonic values at 0.5 ML for the structures with two hollow sites (1906 cm^{-1}) or with two bridge sites (1937 cm^{-1}) is this time more delicate, the calculations show that the observed frequency shift is fully compatible with the hollow site model and can be attributed to increased coverage and adsorbate–adsorbate interactions. The results show that two main phenomena occur when the coverage increases. First the shift caused by static interactions between adsorbates is ruled by the coverage-dependent backdonation from the surface metallic atoms towards the antibonding 2π molecular orbitals of the chemisorbed CO molecules. The second shift is due to dynamic interactions between adsorbates. The stability of a vibrational configuration taken from a particular mode is ruled by the electrostatic energy cost due to the competitive charge transfer between the adsorbates and the metallic surface.

Keywords: Carbon monoxide; Density functional calculations; Low index single crystal surfaces; Palladium; Single crystal surfaces

1. Introduction

Infrared reflection–absorption spectroscopy (IRAS or RAIRS) and high resolution electron energy loss spectroscopy (HREELS) techniques have been traditionally used to perform vibrational spectroscopy of adsorbed molecules on well-defined, single crystal metal surfaces [1]. Additional structure determination can be done with low energy electron diffraction (LEED) or other surface crystallography techniques. The vibrational spectrum of chemisorbed molecules

* Corresponding author; e-mail: sautet@catalyse.univ-lyon1.fr.

0039-6028/99/$ – see front matter
PII: S0039-6028(99)00186-7

allows in many cases the identification of the adsorption state (atomic or molecular) by comparison with the gas-phase spectrum. However, the interpretation of the RAIRS or HREELS spectra seems to be delicate when the determination of the adsorption site is at stake. Although a wide variety of molecules has been already studied on transitional metal surfaces, in some cases the interpretation is not sure [2–4]. A probative case of controversy was established for the $c(4\times2)$ structure of CO on Pd (111). The first procedure proposed by Eischens and Pliskin [5] was to attribute frequency ranges extracted from databases on metal carbonyl complexes. For the supported metals, Ni, Pd and Pt, the high frequency band above 2000 cm^{-1} was attributed to linearly bonded CO and the lower band below 2000 cm^{-1} to bridge-bonded CO. This interpretation of the spectra in terms of 'linear' and 'bridge-bonding' was rejected by Bradshaw and Hoffmann [6] since it did not account for the continuous shift of the IR band during the transition towards high coverage structures. The assignment suggested by Bradshaw and Hoffmann [6] was based on an overview of the spectra from the surfaces (100), (111) and (210). They considered only the absorption band due to isolated CO molecules (singleton) at low coverages as opposed to the domain absorption band at high coverages. Single coordination site (top adsorption) was expected to produce a C–O stretching frequency in the range 2050–2120 cm^{-1}, twofold coordination site (bridge site) was associated with the range 1880–1950 cm^{-1}, and threefold coordination site (hollow site) to 1800–1880 cm^{-1}. Therefore, at a coverage of 0.5 monolayer (ML), the authors assumed from combined LEED and IR measurements, that in the $c(4\times2)$-2 CO structure, the CO molecules must be twofold-coordinated with two bridge sites in the unit cell. This was confirmed by other combined LEED and IRAS studies [7], but was questioned by more recent scanned-energy mode photoelectron diffraction investigations [8] where, in contrast, the structural determination indicates that the CO molecule occupies both hcp and fcc threefold hollow sites.

These discrepancies reveal that the structural determination from vibrational analysis using either the carbonyl complex frequency ranges or the 'singleton method' could lead to erroneous assignments. A correct analysis of the vibrational spectra of adsorbed CO and NO molecules would be helpful for the understanding of the reactivity of three-way catalysts and for the general characterization of the surface sites of catalysts.

Therefore, a detailed density functional theory (DFT) analysis of the relation between C–O stretching frequency and CO adsorption sites on a Pd (111) surface will be presented in this study. The dependence of the C–O stretching vibration on the surface coverage and on the CO–CO molecule vibrational coupling will be discussed.

An extensive range of experimental techniques has been used for the characterization of the molecular adsorption of CO on Pd (111). At least 17 ordered LEED structures have been observed [7]. At low coverage (0.33 ML), a $(\sqrt{3}\times\sqrt{3})R30^{\circ}$-1 CO LEED pattern has been determined [6]. The IR reflection–absorption spectra show a single vibration band at 1836 cm^{-1} [6] that is usually assigned to a threefold fcc hollow adsorption site (the threefold fcc and hcp hollow sites are shown in Fig. 1). This was confirmed by an early dynamical LEED study [9], and recent scanned-energy mode photoelectron diffraction simulations [10]. The transition from $(\sqrt{3}\times\sqrt{3})R30^{\circ}$-1 CO (0.33 ML) to $c(4\times2)$-2 CO (0.5 ML) occurs via a series of ordered overlayers that may be designated $(\sqrt{3}\times n)$rect or $c(\sqrt{3}\times n)$rect where n is an odd integer [11]. This transition is associated with an important shift of $\sim$80 cm^{-1} for the IR band, from 1836 cm^{-1} to either 1918 cm^{-1} [12] or 1920 cm^{-1} [7] for the $c(4\times2)$-2 CO structure. This shift was originally interpreted in terms of a change in the adsorption site from a hollow position to a structure with two bridge-bonded CO molecules [13]. However, a preferred structure with fcc and hcp hollow sites was recently suggested [8,10]. Between the coverages of 0.5 and 0.6 ML, no less than five structures have been observed [7]. Increasing the coverage beyond 0.6 ML produces a series of LEED pattern [14] that, by continuous compression, finally leads to the (2×2)-3 CO high coverage (0.75 ML) struc-

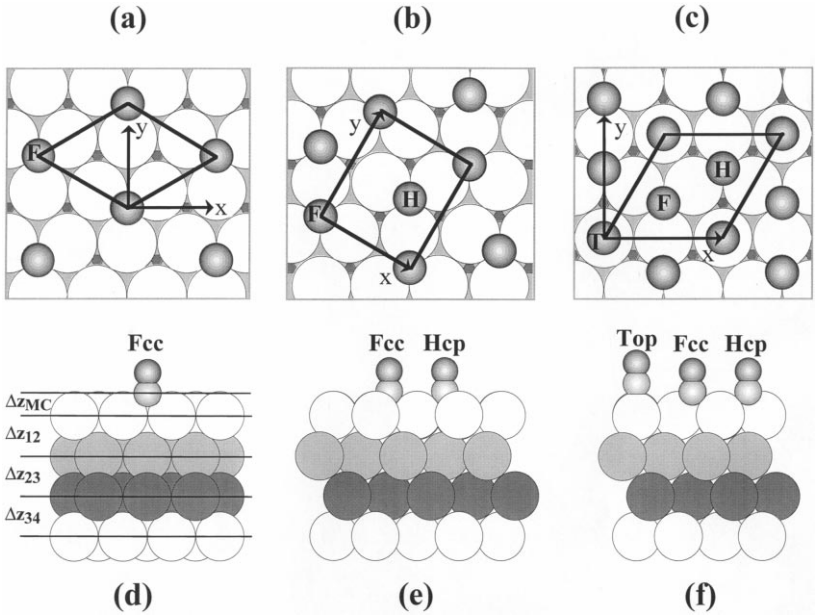

Fig. 1. Most stable adsorption structures of CO on a Pd (111) at coverages: (a) and (d) 0.33 ML, $(\sqrt{3}\times\sqrt{3})$R30°-1 CO (fcc hollow site), (b) and (e) 0.5 ML, c(4×2)-2 CO (fcc and hcp hollow sites), (c) and (f) 0.75 ML, (2×2)-3 CO (top, fcc and hcp hollow sites). (a), (b) and (c) are top views, (d), (e) and (f) are side views. Δz_{MC}, Δz_{12}, Δz_{23} and Δz_{34} are the interlayer spacings used in Table 2. The hcp (fcc) hollow site is above a light-grey second layer (a dark-grey third layer) Pd atom.

ture. The RAIRS spectra show the presence of two single bands: one high frequency band around 2097–2110 cm^{-1} [6,7,12,13,15] and a lower frequency band at 1893–1895 cm^{-1} [6,7,12,13,15]. These peaks have been assigned to a mixture of top and threefold fcc and hcp hollow sites.

The CO chemisorption has been the subject of many theoretical considerations [16–25]. The chemical bonding of CO on metal surfaces was modelled by Blyholder by a Hückel molecular orbital approach [16]. An early effective one electron model Hamiltonian study was performed by Doyen and Ertl [17]. Hoffmann and co-workers carried out extended Hückel calculations on CO chemisorption on several metal surfaces [18–20] and concluded that the previous approach of Blyholder is generally valid, although they emphasized the limitations of such models. Smith and Carter have reported ab initio generalized valence bond and correlation-consistent configuration interaction studies of CO interacting with Pd atoms [21]. The first periodic DFT calculations were performed for the case of CO on Pd (110) [22]. They concluded that the conventional model involving charge donation from CO 5σ states to metal states and backdonation from metal states into 2π states is too simplistic. An extensive ab initio database of CO chemisorption energies calculated within DFT has been reported [23]. Relativistic corrections, implemented by Philipsen et al. in their DFT program [24], show modest effects for the case of CO on Pd (111). Low coverage CO adsorption on finite cluster models of Pd (100) surface has been studied by relativistic gradient-corrected DFT calculations for the top and bridge site adsorptions [25]. The authors have discussed the CO vibrational frequency shifts between Ni, Pd and Pt. To our knowledge, stretching frequency calculations for CO on the Pd (111) surface modelled by a periodic slab, have never been reported. Despite this important theoretical effort, the controversies concerning the preferred adsorption site for the c(4×2)-2 CO structure, the interpretation of vibrational spectra and the description of the chemical bonding, are not yet resolved. So total energy and frequency calcula-

tions can provide an additional contribution for the comparative stability of the surface sites, and for the understanding of the coverage dependence of the C–O stretching vibrations. Another purpose of this study is to propose new frequency ranges for the chemisorption of CO on Pd (111) that could be useful for a better interpretation of the RAIRS spectra.

2. Computational method

2.1. Description of the periodic model

The Pd (111) surface is modelled by a periodic four-layer Pd slab with a CO adlayer on one side of the slab. The $(\sqrt{3}\times\sqrt{3})$R30°-1 CO (0.33 ML), c(4×2)-2 CO (0.5 ML) and (2×2)-3 CO (0.75 ML) structures have been computed. One slab is separated from its periodic image in the z direction by a vacuum space equivalent to five ideal bulk metallic layers. For all structures, the two uppermost Pd layers have been included in the geometry optimisation. The $(\sqrt{3}\times\sqrt{3})$R30°-1 CO structure presents one CO molecule in the unit cell; the four symmetric adsorption site geometries [top, bridge, fcc (Fig. 1a) and hcp hollow sites] have been completely optimised. The c(4×2)-2 CO structure contains two CO molecules per cell; the two bridge-bonded CO system ($2CO_b$) has been optimised and compared with the one fcc and one hcp hollow-bonded CO system (CO_f–CO_b) (Fig. 1b). The (2×2)-3 CO structure has three adsorbed CO molecules in the unit cell. A structure with two bridge and one top CO molecules (CO_t–$2CO_b$) has been optimised and compared with another structure containing a top, an fcc and an hcp hollow CO molecule (CO_t–CO_f–CO_h) (Fig. 1c). For the (CO_t–$2CO_b$) structure, the surface plane degrees of freedom of the C and O atoms have been constrained to the ideal top and bridge positions, because a full relaxation of all the adsorbate coordinates shows that this structure is not energetically stable. Indeed, the full optimisation leads the (CO_t–$2CO_b$) geometry towards the (CO_t–CO_f–CO_h) structure.

The adsorption energy is always averaged upon the different CO molecules in the unit cell. The Pd–Pd interatomic distance has been optimised to 2.80 Å for Pd in the bulk system, and has been used for the frozen part of the model. Tests with the experimental distance parameter of 2.75 Å have been computed and have not shown any influence in the relative energetic stability between the sites.

2.2. Computational details

The geometry optimisations and the C–O stretching vibrations have been performed using the Vienna ab initio simulation program (VASP) [26–28]. The Kohn–Sham equations of the DFT are solved with the generalised gradient approximation (GGA) proposed by Perdew and Wang (e.g. see Ref. [29]). The electron–ion interaction is described by efficient ultrasoft pseudopotentials [30], so that the plane-wave expansion can be truncated at a cut-off energy of 400 eV. Brillouin-zone integrations have been performed on a grid of $7\times7\times1$ Monkhorst–Pack special k-points for the $(\sqrt{3}\times\sqrt{3})$R30°-1 CO structure and $5\times5\times1$ for the c(4×2)-2 CO and (2×2)-3 CO structures. A spin-restricted approach has been used since spin polarisation effects have been found to be negligible [31].

A Mulliken population analysis has been computed for the most stable structures with the Amsterdam density-functional code for periodic structures (ADF-Band) [32,33]. The geometries of the systems have been fixed to the optimum determined by VASP. The metallic slab contains only the two uppermost relaxed layers. The ADF-Band code also solves the Kohn–Sham equations in the density functional framework [34,35], but the main difference is that the wavefunction is developed as a linear combination of localised atomic orbitals. The atoms are modelled by a frozen core up to the 3d orbitals for Pd and up to the 1s orbital for the C and O atoms. Relativistic effects are not included in the calculations, as they were shown to be negligible for palladium slabs [24,36]. The valence basis set (4s 4p 4d 5s for Pd, 2s 2p for O and C) are of double zeta quality for Pd and triple zeta for C and O. The basis set corresponds to a combination of a numerical atomic orbital (NAO) and of Slater-type orbitals (STOs), with an addi-

tional 5p hybridisation orbital for Pd and a 3d polarisation function for C and O. The accuracy for numerical integration was set to 10^{-4}. From 15 to 25 *k*-points were used in the first Brillouin zone.

2.3. Frequency calculation technique

The calculation of the analytic second partial derivatives of the energy of the system are not implemented in VASP. Hence, the C–O stretching calculation needs a numeric exploration of the potential energy surface. Therefore, some approximations are required to simplify the vibrational treatment. Since the C–O stretching vibrations are at a higher frequency than the surface phonons vibrations, the coupling between the C–O stretching and these modes is neglected. The second approximation consists of neglecting the coupling between the adsorbate stretching and bending vibrations for the same reasons.

The metallic slab is fixed to the optimised geometry of the considered chemisorption structure and the C–O bonds are stretched, the centre of mass of the molecule being fixed. The potential energy is fitted over a complete grid of points in the vibrational coordinates (C–O distances). This fit allows one to build the Hessian matrix. The harmonic eigen modes and their associated harmonic wavenumbers are computed by diagonalization of the Hessian matrix. Anharmonic corrections to the harmonic wavenumbers are computed by fitting the potential energy, with Morse-shape potential third-order developments, around the equilibrium state in the space of the normal coordinates. Additional technical details have been given in a previous paper [37].

3. CO chemisorption on a palladium (111) surface

3.1. Energetics and geometry

The gaseous C–O molecule has been computed in a cubic box of $9\times9\times9$ Å^3 size and the C–O distance has been optimised to 1.146 Å. The experimental value is 1.13 Å [38].

For the $(\sqrt{3}\times\sqrt{3})$R30°-1 CO structure (Fig. 1a), the threefold hollow fcc site is the most stable one (Table 1) with an adsorption energy of −2.01 eV, the bridge site being 0.2 eV less stable. This optimal site is in agreement with the experimental interpretation of the vibrational spectra [6] but the calculated adsorption energy values are somewhat larger than the experimental ones of 1.47–1.54 eV [6,39]. The VASP optimised geometry (Table 2 and Fig. 1d) of the system is in very good agreement with the previous LEED analysis of the structure [9,10]. The first interlayer separation Δz_{12}, 2.330 Å (+0.77%) at the Pd surface, is slightly expanded, whereas the second interlayer spacing Δz_{23} (2.295 Å) is very close to the ideal bulk value 2.286 Å.

For the c(4×2)-2 CO structure (Fig. 1b), the CO_f–CO_h model is favoured (with an average CO adsorption energy of −1.85 eV). The $2CO_b$ model is 0.06 eV per CO molecule higher in energy. Optimisations with the experimental Pd–Pd distance parameter of 2.75 Å do not modify the energy order and $2CO_b$ is less stable by 0.07 eV per CO molecule. This result agrees with a recent scanned-energy mode photoelectron diffraction study [8] and contrasts with the original interpretation of the IR spectra that concluded to the existence of the $2CO_b$ structure [6,7]. At medium coverage (0.5 ML) the adsorption energy per CO molecule is weaker than the one at low coverage (0.33 ML). The optimised geometry (Table 2) agrees well with the recent XPD determination [8]. The C–O distances seem to be slightly overestimated at the GGA level. The first interlayer spacing Δz_{12} (Table 2) is expanded (+0.9%).

For the (2×2)-3 CO model (Fig. 1c and f), the CO_t–CO_f–CO_h model is found to be more stable (−1.46 eV per CO) than the CO_t–$2CO_b$ model (−0.97 eV per CO). This complies with what was interpreted experimentally from the vibrational analysis [6,7,12,13,15]. Once again the adsorption energy has been weakened in going from a coverage of 0.5 ML to 0.75 ML. The expansion of the first interlayer spacing Δz_{12} increases with CO coverage (+1.02% for the CO_t–CO_f–CO_h model).

3.2. Vibrational analysis

The IR experimental assignment of the c(4×2)-2 CO structure, based on the comparison

Table 1
Adsorption energies E_{ads} (eV), anharmonic ν_{anharm} and scaled anharmonic $1.027 \times \nu_{anharm}$. C–O stretching frequencies (cm^{-1}) for the chemisorption of CO on Pd (111), at coverages 0.33 ML [$(\sqrt{3} \times \sqrt{3})R30^{\circ}$-1 CO], 0.5 ML [c(4×2)-2 CO] and 0.75 ML [(2×2)-3 CO]. For the c(4×2)-2 CO and the (2×2)-3 CO structures, the exponents on the CO bond lengths correspond to the adsorption site: (b) bridge site; (f) fcc hollow site; (h) hcp hollow site; (t) top site. The infrared active modes are marked with an asterisk

Structure	$(\sqrt{3} \times \sqrt{3})R30^{\circ}$-1 CO				c(4×2)-2 CO		(2×2)-3 CO		Gas
Coverage	$\theta = 0.33$ ML				$\theta = 0.5$ ML		$\theta = 0.75$ ML		phase
Sites	Top	Bridge	Hollow hcp	Hollow fcc	2 bridge	Fcc+hcp	Top+2 bridge	Top+fcc+hcp	
d_{C-O} (Å)	1.157	1.178	1.188	1.189	1.175(b)	1.182(f)	1.146(t)	1.151(t)	1.146
					1.175(b)	1.182(h)	1.188(b)	1.183(f)	
							1.184(b)	1.182(h)	
E_{ads} (eV)	−1.36	−1.81	−1.98	−2.01	−1.79	−1.85	−0.97	−1.46	
ν_{anharm} (cm^{-1})									
ν_1	2014	1848	1781	1779	1885	1856	2052	2030	2087
$1.027 \times \nu_1$	2069	1898	1830	1828*	1937	1906*	2107	2085*	2143
ν_2					1838	1801	1831	1843	
$1.027 \times \nu_2$					1888	1850	1881	1893*	
ν_3							1766	1786	
$1.027 \times \nu_3$							1814	1835	
ν_{Exp} (cm^{-1})	1836[a]				1918[b]; 1920[c]		2097[b]; 2110[c]		2143[d]
							1893[b]; 1894[c]		

[a] Ref. [6].
[b] Ref. [12].
[c] Ref. [7].
[d] Ref. [40].

Table 2
Optimised C–O bond lengths d_{CO}, mean C–Surface distance Δz_{MC}, and mean palladium interlayer spacings (Fig. 1) Δz_{12}, Δz_{23}, and Δz_{34} for adsorbed CO on Pd (111). The most stable structures are considered: at low coverage $(\sqrt{3} \times \sqrt{3})R30^{\circ}$-1 CO 0.33 ML with a threefold fcc hollow CO adsorbate (F); at medium coverage c(4×2)-2 CO 0.5 ML with both threefold fcc (F) and hcp (H) hollow CO adsorbates; high coverage (2×2)-3 CO 0.75 ML with top (T), fcc (F) and hcp (H) hollow CO adsorbates in the structure

Structure	$(\sqrt{3} \times \sqrt{3})R30^{\circ}$-1 CO			c(4×2)-2 CO		(2×2)-3 CO
Sites	Hollow fcc			Hollow fcc+hcp		Top+fcc+hcp
	This work	[9]	[10]	This work	[8]	This work
d_{CO}(F) (Å)	1.189	1.15±0.05	1.25+0.14/−0.11	1.182	1.14±0.12	1.183
d_{CO}(H) (Å)				1.182	1.14±0.14	1.182
d_{CO}(T) (Å)						1.151
Δz_{MC}(F) (Å)	1.296	1.29±0.05	1.27±0.05	1.366	1.31±0.06	1.366
Δz_{MC}(H) (Å)				1.373	1.37±0.06	1.373
Δz_{MC}(T) (Å)						1.901
Δz_{12} (Å)	2.330	2.386±0.05		2.345		2.351
Δz_{23} (Å)	2.295	2.246±0.05		2.292		2.292
Δz_{34} (Å)	2.286			2.286		2.286

with the C–O stretching frequency ranges of the carbonyl transition metal complexes or with the 'singleton method', suggests the presence of a structure containing two bridge sites, whereas the XPD experiments and the DFT–VASP computations indicate that the model with the fcc and hcp

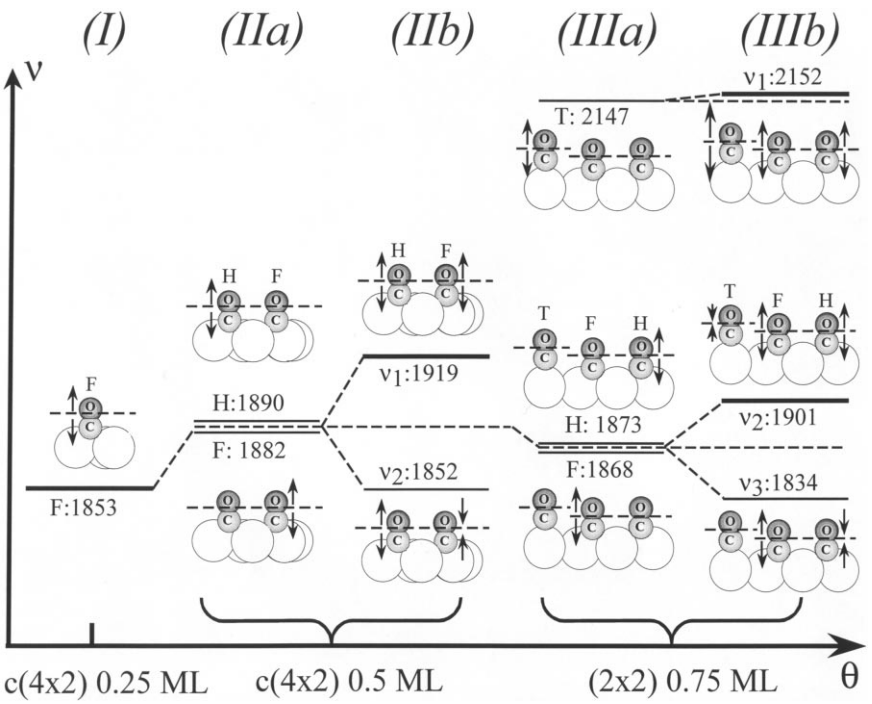

Fig. 2. Dependence of the scaled ν(C–O) stretching harmonic wavenumbers (cm^{-1}) on the coverage for the chemisorption of CO on Pd (111) surfaces. (I) At coverage 0.33 ML [$(\sqrt{3}\times\sqrt{3})$R30°-1 CO, fcc hollow site]; (IIa) uncoupled modes at coverage 0.5 ML [$c(4\times2)$-2 CO, fcc and hcp hollow sites]; (IIb) coupled modes ν_1 and ν_2 at coverage 0.5 ML [$c(4\times2)$-2 CO, fcc and hcp hollow sites]; (IIIa) uncoupled modes at coverage 0.75 ML [(2×2)-3 CO, top, fcc and hcp hollow sites]; (IIIb) coupled modes ν_1, ν_2 and ν_3 at coverage 0.75 ML [(2×2)-3 CO, top, fcc and hcp hollow sites]. The sites are indicated by the following letters: T for top site, F for fcc hollow site and H for hcp hollow site.

hollow sites is favoured. The blue shift of the band around 1840 cm^{-1} at coverage 0.33 ML towards 1920 cm^{-1} at 0.5 ML has been generally considered as a change of site from the threefold hollow to the twofold bridge adsorption. In order to clear this discrepancy, C–O stretching wavenumbers have been calculated for all the sites of the $(\sqrt{3}\times\sqrt{3})$R30°, $c(4\times2)$ and (2×2) structures.

Table 1 presents the calculated anharmonic wavenumbers for the CO chemisorption on Pd surfaces for all the different stretching vibration modes. Only the wavenumbers associated with the highest symmetric modes are supposed to be infrared active and, therefore, their corresponding anharmonic values are marked with an asterisk.

For the gaseous CO molecule we obtain a harmonic stretching wavenumber of 2112 cm^{-1}. This is ~3% smaller than the experimental value of 2170 cm^{-1} [38]. The anharmonic frequency 2087 cm^{-1} is also smaller than the experimental value of 2143 cm^{-1} [40]. Therefore, the computed wavenumbers will be considered as slightly softer than the experimental IR ones. Hence, all the calculated frequencies have been scaled by 1.027 (chosen such that the gas-phase calculated CO stretching frequency equals the corresponding observed value) as clearly indicated in Table 1. In Fig. 2 the scaled *harmonic* frequencies are presented for coupled and uncoupled modes as a function of coverage because the uncoupled modes are determined only at the *harmonic* level in the Hessian matrix.

For the $(\sqrt{3}\times\sqrt{3})$R30°-1 CO model (0.33 ML), the scaled anharmonic frequency for the preferred fcc hollow site is 1828 cm^{-1} (Table 1). The experimental value, 1836 cm^{-1} [6], is in a good agreement with the calculated fcc hollow site frequency and is clearly different from the bridge site

result, which lies significantly higher in frequency (1898 cm^{-1}).

The c(4 × 2)-2 CO structure (0.5 ML) contains two CO molecules in the unit cell. Hence, we have obtained two eigen modes: the ν_1 mode (highest frequency), which is related to a symmetric vibration of the two chemisorbed CO molecules (Fig. 2IIb, with a scaled harmonic frequency of 1919 cm^{-1}); the ν_2 mode, which is associated with an antisymmetric vibration of the adsorbates (Fig. 2IIb, with a scaled harmonic frequency of 1852 cm^{-1}). The scaled anharmonic ν_1 wavenumbers are 1906 cm^{-1} for CO_f–CO_h and 1937 cm^{-1} for $2CO_b$ (Table 1). The scaled anharmonic ν_2 frequencies are 1850 cm^{-1} for CO_f–CO_h and 1888 cm^{-1} for $2CO_b$ (Table 1). The splitting between the two modes ($\sim$50–60 cm^{-1}) results from vibrational coupling. The largest variation of the electric dipole moment perpendicular to the surface is clearly involved in the ν_1 mode. As a direct consequence, its infrared activity is presumably the highest. The experimental values, 1918–1920 cm^{-1} [7,12], fall between the two calculated anharmonic values for the ν_1 mode. So the comparison is more delicate. However, the frequency blue shift of 80 cm^{-1} observed experimentally between 0.33 and 0.5 ML does not necessarily have to be linked to a change of the chemisorption site from a hollow to a bridge position, but is fully compatible with a conservation of the hollow site as suggested from the total energy calculations and XPD results. So the shift should not be interpreted as a change of the site but it is most probably due to the increasing coverage effect. This will be discussed in detail below.

For the (2 × 2)-3 CO structure (0.75 ML) the unit cell has three CO molecules. The vibrational treatment reveals three distinct eigen modes: ν_1 (highest frequency), ν_2 and ν_3 (Fig. 2IIIb, with respective scaled harmonic frequencies of 2152 cm^{-1}, 1901 cm^{-1} and 1834 cm^{-1}). The highest mode is totally symmetric and mainly developed on the top site CO. In the ν_2 mode, the two fcc and hcp hollow-bonded CO molecules (or two bridge-bonded CO) vibrate symmetrically. This mode presents a small out-of-phase component for the top site CO. The ν_3 mode corresponds to an antisymmetric displacement of the hollow or the bridge sites and a very small component for the top site. For the most stable CO_t–CO_f–CO_h model, the calculated scaled ν_1 and ν_2 values (2085 cm^{-1} and 1893 cm^{-1} respectively in Table 1) agree with the experimental ranges 2097–2110 cm^{-1} and 1893–1895 cm^{-1} [6,7,12,13,15].

4. Molecular orbital analysis

4.1. Dependence of stretching frequency on the surface coverage

The dependence of the C–O stretching frequency on the surface coverage and adsorbate–adsorbate interactions is presented in Fig. 2. In this frequency diagram the scaled *harmonic* wavenumbers are reported as a function of coverage only for the most stable structures. The values are associated to full segments, the IR active bands being indicated by bold segments. At low coverage ($\sqrt{3} \times \sqrt{3}$)R30°-1 CO 0.33 ML or c(4 × 2)-1 CO 0.25 ML (Fig. 2I), there is one stretching frequency at 1853 cm^{-1} for the favoured fcc hollow adsorption. When the coverage increases from 0.25 or 0.33 ML to 0.5 ML, another molecule adsorbs in the unit cell of the c(4 × 2) structure on a hcp hollow position. The calculation of the uncoupled vibrations of the two CO molecules shows two uncoupled modes that are close to a mean value around 1886 cm^{-1} (Fig. 2IIa), so the band has been blue shifted by 30 cm^{-1}. This first blue shift is only caused by a change of the coverage, not a vibrational coupling, since only one molecule is allowed to vibrate. We will call it the 'static effect'. In a second step (Fig. 2IIb), the calculation of harmonic normal modes takes into account the coupling of the two CO vibrational movements. The coupling is rather strong ($\sim$70 cm^{-1}) and it leads to an important broadening of the band (Fig. 2IIb) around the mean value of 1886 cm^{-1}. The symmetric vibration ν_1 of the two hollow-bonded CO is shifted by 33 cm^{-1} towards the top of the band (1919 cm^{-1}), whereas the antisymmetric mode ν_2 is pushed down by 34 cm^{-1} to the bottom of the band (1852 cm^{-1}). This second shift is due to the adsorbate–adsorbate vibrational cou-

pling, and will be called the 'dynamic effect'. At high coverage (2×2)-3 CO 0.75 ML, a third top CO molecule is added in the structure. The calculated frequencies of the uncoupled harmonic modes are reported in Fig. 2IIIa. The low frequency mean band of the fcc and hcp hollow-bonded CO molecules is red shifted from 1886 cm^{-1} to 1870 cm^{-1}. A second high frequency band, due to the independent vibration of the top CO, appears at 2147 cm^{-1}. The coupling of the three CO stretches induces a large splitting of the low frequency band, equivalent to the previous broadening at 0.5 ML, and a small blue shift of the high frequency band (Fig. 2IIIb). The coupling is obviously stronger when the stretching vibrations are close in frequency. The two hollow site symmetric mode ν_2 is blue shifted by 31 cm^{-1} from the mean band, and the antisymmetric mode ν_3 is red shifted by also 36 cm^{-1}.

4.2. Interpretation of the static effect

The shifts, first blue then red, of the mean hollow band due to the increased coverage can be explained by a comparative analysis of the Mulliken populations of the fcc and hcp hollow CO for all the structures. In Table 3 we have reported the electronic populations of the important molecular orbitals of the fcc hollow-bonded CO molecule for the most stable structures at coverages 0.33, 0.5 and 0.75 ML. The total electronic populations are also given for the CO molecules and for the surface Pd atoms.

When the coverage increases from 0.33 to 0.5 ML, the CO molecule loses 0.1 electron on average (Table 3). The backdonation from the metallic surface to the antibonding $2\pi_x$(fcc) and $2\pi_y$(fcc) molecular orbitals (not populated in the gas-phase CO molecule) is lowered (from 0.296 to 0.249 and 0.147 respectively) at coverage 0.5 ML, so the C–O bond is strengthened. The degeneracy between $2\pi_x$(fcc) and $2\pi_y$(fcc) is lost because there is no C_3 axis in the symmetry group of the $c(4\times2)$ structure. This accounts for the difference in their electronic populations. Let us examine the projected densities of states (PDOS) on $2\pi_y$ for fcc CO (Fig. 3). The zero energy value is the Fermi level. The integration of the PDOS at the Fermi level gives the electronic population of the molecular orbital. In Fig. 3 the low-lying band between -5.5 and -6 eV comes from the mixing with the bonding 1π molecular orbitals through the metallic d band. The band between -4 eV and the Fermi level, corresponds to the part of the 2π molecular orbitals that is populated by interaction with the metallic d band. Beyond the Fermi level, the vacant states are mainly developed on the 2π molecular orbitals. At 0.5 ML, the stabilized part of 2π

Table 3
Mulliken electronic populations of the $1\pi_x$, $1\pi_y$, 5σ, $2\pi_x$ and $2\pi_y$ molecular orbitals of the fcc hollow CO; total electronic populations for the fcc, hcp hollow and top CO molecules (and their average value), for the surface Pd atom (average value) in the most stable structures $(\sqrt{3}\times\sqrt{3})$R30°-1 CO 0.33 ML (fcc hollow), $c(4\times2)$-2 CO 0.5 ML (fcc and hcp hollow) and (2×2)-3 CO 0.75 ML (top, fcc and hcp hollow) of CO on Pd (111)

Structure	$(\sqrt{3}\times\sqrt{3})$R30°-1 CO	$c(4\times2)$-2 CO	(2×2)-3 CO
Coverage	0.33 ML	0.5 ML	0.75 ML
Sites	Fcc hollow	Fcc and hcp hollow	Top, fcc and hcp hollow
$1\pi_x$ (CO fcc)	1.936	1.938	1.943
$1\pi_y$ (CO fcc)	1.936	1.959	1.944
5σ (CO fcc)	1.516	1.497	1.488
$2\pi_x$ (CO fcc)	0.296	0.249	0.261
$2\pi_y$ (CO fcc)	0.296	0.147	0.261
CO (fcc)	9.940	9.837	9.885
CO (hcp)		9.857	9.900
CO (top)			9.650
CO (average)	9.940	9.847	9.812
Surface Pd atom (average)	17.966	17.975	17.987

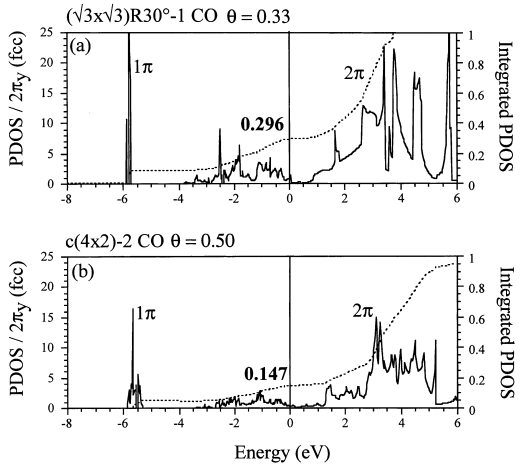

Fig. 3. Projected densities of states (PDOS) for fcc hollow-bonded CO on a two-layer Pd (111) surface as a function of coverage; projection on: (a) the CO $2\pi_y$ molecular orbital at coverage 0.33 ML $(\sqrt{3}\times\sqrt{3})$R30°-1 CO; (b) the CO $2\pi_y$ molecular orbital at coverage 0.50 ML c(4×2)-2CO (x and y directions are given in Fig. 1). The dotted lines are the integrations of the PDOS. The zero on the energy axis corresponds to the Fermi level. The value of the integrated PDOS at the Fermi level indicates the electronic occupation of the molecular orbital.

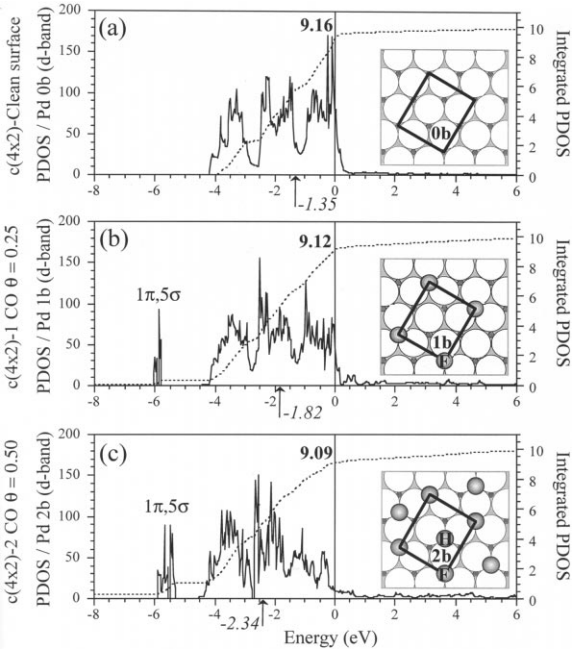

Fig. 4. Projected densities of states (PDOS) for hollow-bonded CO on a two-layer Pd (111) surface as a function of coverage; projection on: (a) the surface Pd '0b' d-band for a clean surface c(4×2); (b) the surface Pd '1b' d-band at coverage 0.25 ML c(4×2)-1 CO; (c) on the surface Pd '2b' d-band at coverage 0.5 ML c(4×2)-2 CO. In each case, a figure indicates the position of the Pd atom, '0b', '1b' and '2b' in the unit cell, with CO molecules in: (b) an fcc hollow site (F), (c) fcc and hcp hollow sites (F and H). The dotted lines are the integrations of the PDOS. The zero on the energy axis corresponds to the Fermi level. The value of the integrated PDOS at the Fermi level indicates the electronic occupation of the molecular orbital. The vertical arrows between −1 and −3 eV correspond to the mean energy band position of each projection.

molecular orbitals is reduced (Fig. 3a and b) mainly because there is a decrease of the interaction with the d-band below the Fermi level. The PDOS on the d orbitals of a surface Pd atom that is directly bonded to an fcc hollow CO molecule is presented in Fig. 4. In order to understand how the chemisorption of CO perturbs the metal, we have plotted the d-band PDOS for the clean surface (Fig. 4a), for the c(4×2)-1 CO structure (fcc hollow, Fig. 4b) and for the c(4×2)-2 CO structure (Fig. 4c). The position of the metal atom in the unit cell is indicated for each structure (Pd non-bonded with CO '0b' in Fig. 4a, Pd onefold coordinated with CO '1b' in Fig. 4b, and Pd twofold coordinated with CO '2b' in Fig. 4c). At zero coverage, the d-band appears between −4.25 and +0.5 eV (Fig. 4a). The mean energy position of the band is indicated with a vertical arrow at −1.35 eV below the Fermi level. When the coverage increases to 0.25 ML, the Pd '1b' d-bands present new peaks at −6 eV that account for the interaction with the fcc hollow CO 5σ and 1π molecular orbitals. The interactions between the d-band and the CO 2π band causes a shift of −0.47 eV in the mean d-band energy position, from −1.35 to −1.82 eV. The strong backdonation from the metal d-band towards the CO 2π molecular orbitals results in an important depopulation of the high energy d-band states and a change of the shape of the d-band. The Pd atom interacting with one CO molecule shows d states that are in average lower in energy and has therefore reduced capabilities to induce new back bonding interactions with a second CO molecule. This trends is enhanced when a second molecule is adsorbed in the hcp hollow position, with a shift to −2.34 eV of the average band energy and a

strong depletion of d states in the vicinity of the Fermi level. The two CO molecules compete for backbonding interactions and the electronic transfer towards 2π for one molecule is reduced, as seen in Table 3. As a result, the CO bond is strengthened and the stretching frequency increases from 1853 to 1882 cm^{-1} (Fig. 2I and IIa).

The increase of the donation of the 5σ molecular orbital to the surface (Table 3) has no influence on the strength of the CO bond because the 5σ MO is mainly C–O non-bonding.

If a higher coverage of 0.75 ML is considered, the competition for backbonding interactions is even stronger and the average CO electronic population is even further decreased. However, the three CO molecules are not equivalent in the unit cell. It is also well known that the top site CO adsorption is not as favourable as the hollow site position for backbonding [20,41,42], so the transfer towards 2π molecular orbitals is smaller for top CO molecules. As a consequence, the backdonation is lightly enhanced for the two other fcc and hcp hollow site CO molecules, with a small gain of 0.04 electron compared with the 0.5 ML situation. The C–O bond is hence slightly weakened and this explains the stretching frequency decrease for the hollow site CO at 0.75 ML (from 1882 to 1868 cm^{-1} in Fig. 2IIa and IIIa).

4.3. Interpretation of the dynamic effect

The strong vibrational coupling between hollow site CO stretching modes at coverages 0.5 and 0.75 ML can be interpreted with a Mulliken electronic population variation analysis. In Fig. 5 we have reported the charge transfers for the fcc and hcp hollow CO molecules and the metallic surface in the c(4 × 2)-2 CO 0.50 ML structure for two distinct vibrational configurations. The references are the electronic populations of the energy minimum. The first configuration is related to an antisymmetric vibration associated with the ν_2 vibration mode. The elongation of 0.05 Å of the fcc hollow C–O bond is followed by an electronic gain of 0.047 electron, whereas the shortening of 0.05 Å of the hcp hollow C–O bond involves an electronic loss of 0.045 electron. These important transfers are represented with double curved arrows in Fig. 5. The surface, which plays here the role of an electronic reservoir, participates in the transfer without being affected (−0.003 electron). In the second configuration both fcc and hcp CO are elongated. By transferring an equivalent quantity of 0.015 electron to each CO molecule (single curved arrows), the surface loses more electrons (−0.051 electron) and is therefore strongly affected by the symmetric vibrations of the two adsorbates. The additional energetic cost for the symmetric vibration has been estimated to be +0.148 eV (Fig. 5) with the ADF-Band program with respect to the antisymmetric vibration. The energy variation between the equilibrium configuration and the symmetric and antisymmetric displacements may be modelled by a crude decomposition in elastic and electrostatic contributions. The quadratic elastic energy term takes into account the bond energy variation during the C–O stretching. This term is identical in both symmetric and antisymmetric configurations, since the amplitude of bond length variations is the same. The electrostatic energy term has been computed as a Madelung calculation for the two vibrational configurations with ADF-Band Mulliken charges centred on the positions

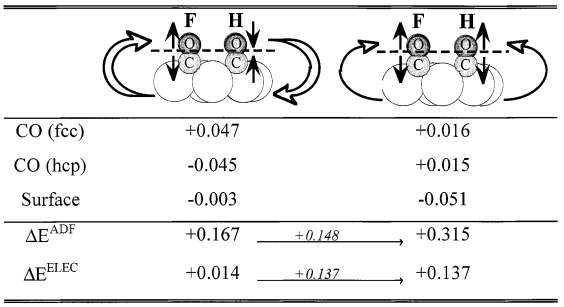

Fig. 5. ADF-Band electronic population variations for the fcc and hcp hollow CO adsorbates, and for the metallic surface in the case of the c(4 × 2)-2 CO 0.5 ML structure on Pd (111) as a function of the symmetric or antisymmetric CO vibrational configurations. The electronic population reference is that of the energy minimum reported in Table 3. The curved arrows of the stretching configurations show the direction of the electronic transfer. An important transfer appears with a double arrow; a small transfer with a single arrow. The total energy difference ΔE^{ADF} (eV) obtained by the ADF-Band program and the electrostatic energy difference ΔE^{ELEC} (eV) obtained with a Madelung calculation are indicated for the symmetric and the antisymmetric vibrational configurations (the energy reference being the equilibrium state).

of the Pd, C and O atoms in the unit cell. This second term has been estimated to be +0.014 eV for the antisymmetric mode (Fig. 5) and +0.137 eV for the symmetric vibration (the reference being the equilibrium state). So the calculated electrostatic energy difference between the symmetric and the antisymmetric configurations has been estimated to be +0.123 eV. This, therefore, accounts qualitatively for the total energetic cost of +0.148 eV. Hence, elongating one CO while shortening the other is energetically more favourable than simultaneously elongating both CO. Thus the antisymmetric vibration is associated with a mode that is softer than the non-coupled situation and the symmetric vibration to a harder mode. The strong coupling between hollow site CO molecules at 0.75 ML can be explained similarly.

5. Conclusion

Stretching frequency calculations for the chemisorption of CO on the Pd (111) surface have been reported for the first time with a detailed coverage-dependent periodic DFT approach. Three distinct coverages have been studied. The energetic results indicate that the fcc and hcp hollow sites are always favoured for this surface. When the coverage increases, the adsorbed CO molecule becomes less stable on Pd (111). These trends follow previous DFT results for the chemisorption of NO on Pd and Rh (111) surfaces [31,37]. At a low coverage of 0.33 ML and a high coverage of 0.75 ML, the results show that the most stable structures are the ones containing threefold fcc and hcp hollow sites (together with a top site CO at 0.75 ML). They agree with previous LEED and IR experiments. The calculated anharmonic frequencies match the experimental IR bands extracted from the vibrational spectra. At a medium coverage of 0.5 ML the most stable structure is the one with both fcc and hcp hollow sites, in contrast with the usual interpretation of the IR spectra concluding to a favoured two bridge structure. The important shift to higher frequency between 0.33 and 0.5 ML can be fully explained by the increased coverage and does not have to be associated with a change of the site of the molecule. An effort has been made in this work to clear the obvious disagreement between calculations and interpretation procedures of the spectra by presenting the dependence of the C–O stretching wavenumbers on the surface coverage. The analysis points out that the coverage dependence of the frequency is ruled by two main effects. The first effect comes from static interactions between neighbouring adsorbates. When the coverage changes, the blue or red shift of the threefold hollow site mean frequency band is directly linked to the competitive backdonation from the metallic surface to the 2π molecular orbitals of the hollow-bonded CO molecules. The second effect is due to dynamic vibrational coupling between adsorbates. When the CO molecules are stretched on the surface according to different vibrational modes, the stability of the configuration strongly depends on the electrostatic energy cost of the charge transfer between the metallic surface and the adlayer.

Acknowledgements

This work has been undertaken within the GdR–Dynamique Moléculaire Quantique Appliquée à la Catalyse, Centre National de la Recherche Scientifique, Technische Universität Wien, Institut Français du Pétrole and TOTAL. The authors want to thank IDRIS at CNRS for the attribution of CPU time (Project No. 980016).

References

[1] F.M. Hoffmann, Surf. Sci. Rep. 3 (1983) 107.
[2] P.J. Chen, D.W. Goodman, Surf. Sci. 297 (1993) L93.
[3] H.J. Borg, J.F.C.-J.M. Reijerse, R.A. van Santen, J.W. Niemantsverdriet, J. Chem. Phys. 101 (1994) 10052.
[4] N. Materer, A. Barbieri, D. Gardin, U. Starke, J.D. Batteas, M.A. Van Hove, G.A. Somorjai, Surf. Sci. 303 (1994) 319.
[5] R.P. Eischens, W.A. Pliskin, Adv. Catal. 10 (1958) 1.
[6] A.M. Bradshaw, F.M. Hoffmann, Surf. Sci. 72 (1978) 513.
[7] M. Tüshaus, W. Berndt, H. Conrad, A.M. Bradshaw, B. Persson, Appl. Phys. A 51 (1990) 91.
[8] T. Gießel, O. Schaff, C.J. Hirschmugl, V. Fernandez, K.-M. Schindler, A. Theobald, S. Bao, R. Lindsay, W.

Berndt, A.M. Bradshaw, C. Baddeley, A.F. Lee, R.M. Lambert, D.P. Woodruff, Surf. Sci. 406 (1998) 90.
[9] H. Ohtani, M.A. van Hove, G.A. Somorjai, Surf. Sci. 187 (1987) 372.
[10] V. Fernandez, T. Gießel, O. Schaff, K.-M. Schindler, A. Theobald, C.J. Hirschmugl, S. Bao, A.M. Bradshaw, C. Baddeley, A.F. Lee, R.M. Lambert, D.P. Woodruff, V. Fritzsche, Z. Phys. Chem. 198 (1997) 73.
[11] M. Tüshaus, W. Berndt, D. Hoge, A.M. Bradshaw, in preparation.
[12] A. Ortega, Thesis, Freie Universität Berlin, 1980.
[13] J. Szanyi, W.K. Kuhn, D.W. Goodman, J. Vac. Sci. Technol. A: 11 (1993) 1969.
[14] H. Conrad, Thesis, Universität, München, 1976.
[15] W.K. Kuhn, J. Szanyi, D.W. Goodman, Surf. Sci. 274 (1992) L611.
[16] G. Blyholder, J. Phys. Chem. 68 (1964) 2772.
[17] G. Doyen, G. Ertl, Surf. Sci. 69 (1977) 157.
[18] S.-S. Sung, R. Hoffmann, J. Am. Chem. Soc. 107 (1985) 578.
[19] J. Li, B. Schiott, R. Hoffmann, D.M. Proserpio, J. Phys. Chem. 94 (1990) 1554.
[20] Y.-T. Wong, R. Hoffmann, J. Phys. Chem. 95 (1991) 859.
[21] G.W. Smith, E.A. Carter, J. Phys. Chem. 95 (1991) 2327.
[22] P. Hu, D.A. King, M.-H. Lee, M.C. Payne, Chem. Phys. Lett. 246 (1995) 73.
[23] B. Hammer, Y. Morikawa, J.K. Nørskov, Phys. Rev. Lett. 76 (1996) 2141.
[24] P.H.T. Philipsen, E. van Lenthe, J.G. Snijders, E.J. Baerends, Phys. Rev. B 56 (1997) 13556.
[25] G. Pacchioni, S.-C. Chung, S. Krüger, N. Rösch, Surf. Sci. 392 (1997) 173.
[26] G. Kresse, J. Hafner, Phys. Rev. B 47 (1993) 558.
[27] G. Kresse, J. Hafner, Phys. Rev. B 48 (1993) 13115.
[28] G. Kresse, J. Hafner, Phys. Rev. B 49 (1994) 14251.
[29] J.P. Perdew, J.A. Chevary, S.H. Vosko, K.A. Jackson, M.R. Pederson, D.J. Singh, C. Fiolhais, Phys. Rev. B 46 (1992) 6671.
[30] D. Vanderbilt, Phys. Rev. B 41 (1990) 7892.
[31] D. Loffreda, D. Simon, P. Sautet, J. Chem. Phys. 108 (1998) 6447.
[32] ADF-Band package, Laboratory of Theoretical Chemistry, Free University Amsterdam, Netherlands.
[33] G. te Velde, E.J. Baerends, Phys. Rev. B 44 (1991) 7888.
[34] P. Hohenberg, W. Kohn, Phys. Rev. B 136 (1964) 864.
[35] W. Kohn, L.J. Sham, Phys. Rev. A 140 (1965) 1113.
[36] S.-C. Chung, S. Krüger, G. Pacchioni, N. Rösch, J. Chem. Phys. 102 (1995) 3695.
[37] D. Loffreda, D. Simon, P. Sautet, Chem. Phys. Lett. 291 (1998) 15.
[38] K. Nakamoto, Infrared and Raman Spectra of Inorganic and Coordination Compounds, 4th edition, Wiley, New York, 1986.
[39] X. Guo, J.T. Yates Jr,, J. Chem. Phys. 90 (1989) 6761.
[40] S.-I. Ishi, Y. Ohno, B. Viswanathan, Surf. Sci. 161 (1985) 349.
[41] F. Delbecq, B. Moraweck, L. Vérité, Surf. Sci. 396 (1998) 156.
[42] F. Delbecq, P. Sautet, Phys. Rev. B submitted for publication.